Published online in advance by J-STAGE

J Prosthodont Res. 2022; **(**): ****–****

OPEN ACCESS JPR Prosthodontic Research

Journal of Prosthodontic Research

Original article

# Fracture behavior of discontinuous fiber-reinforced composite inlay-retained fixed partial denture before and after fatigue aging

Lippo Lassila[a], Enas Mangoush[a,*], Pekka K. Vallittu[a,b], Sufyan Garoushi[a]

[a]Department of Biomaterials Science and Turku Clinical Biomaterials Centre -TCBC Institute of Dentistry, University of Turku, Turku, Finland

[b]City of Turku Welfare Division, Oral Health Care, Turku, Finland

**Abstract**

**Purpose:** To evaluate the fracture behavior of inlay-retained fixed partial dentures (IRFPDs) made of experimental short fiber-reinforced composite (SFRC) computer-aided design/computer-aided manufacturing (CAD/CAM) block before and after cyclic fatigue aging.

**Methods:** Five groups (n=20/group) of three-unit posterior IRFPDs were fabricated. The first and second groups were CAD/CAM fabricated from experimental SFRC blocks or lithium-disilicate (IPS e.max CAD, IVOCLAR) materials, the third group comprised a three-dimensional-printed composite (Temp PRINT, GC), and the fourth and fifth groups comprised conventional laboratory flowable composite (Gradia Plus, GC) and commercial flowable SFRC (everX Flow, GC), respectively. All IRFPDs were luted into a metal jig with adhesive dual-cure resin cement (RelyX Ultimate, 3M ESPE). Half the IRFPDs per group (n=10) were subjected to fatigue aging for 10,000 cycles. The remaining half were statically loaded until fracture without fatigue aging. The load was applied vertically between triangular ridges of the buccal and lingual cusps. The fracture mode was visually examined using optical and scanning electron microscopy (SEM). Data were statistically analyzed using a two-way analysis of variance (ANOVA) followed by Tukey's HSD test.

**Results**: ANOVA revealed that IRFPDs made of experimental SFRC CAD/CAM had the highest ($p$<0.05) load-bearing capacity before (2624±463 N) and after (2775±297 N) aging among all groups. Cyclic fatigue aging decreased the load-bearing capacity ($p$>0.05) of all tested prostheses, except for the experimental SFRC CAD/CAM and conventional laboratory composite IRFPDs ($p$>0.05). SEM images showed the ability of discontinuous short fibers in the experimental SFRC CAD/CAM composite to redirect and hinder crack propagation.

**Conclusion:** CAD/CAM-fabricated IRFPDs made of experimental SFRC blocks showed promising performance in clinical testing in terms of fracture behavior.

**Keywords:** Fracture behavior, CAD/CAM restoration, inlay-retained fixed partial denture, fatigue aging, short fiber composite

Received 18 February 2022, Accepted 15 June 2022, Available online 28 July 2022

## 1. Introduction

A wide variety of restorative techniques and materials are available to restore a single missing tooth, ranging from conventional crown-retained fixed partial dentures (FPDs) to dental implants[1].

As the need for conservative treatment options with minimal tooth preparation is growing, interest in resin-bonded FPDs with partial coverage retainers, such as surface or inlay-retained FPDs, has increased. These dentures can preserve the intact tooth structure with minimal intervention[2], and patients can avoid surgical procedures and high costs of dental implants. However, partial-coverage restorations may have an increased risk of fracture and de-bonding as they are smaller than complete coverage substitutes[3]. Continuous progress in processing technologies and material properties is an attempt to overcome these drawbacks. Therefore, proper selection of the restorative material is essential, especially in the posterior region, as the material of choice plays a crucial role in the biomechanical distribution of stresses and, subsequently, the clinical longevity of the restoration[4].

The most commonly used materials for fabricating inlay retained fixed partial dentures (IRFPDs) are metal ceramics, all-ceramics, and composites[3]. Despite the favorable performance of metal-ceramic IRFPDs, these restorations have some drawbacks, such as reduced translucency, ceramic chipping, and debonding between the metal and overlying ceramics. Consequently, other materials can achieve a certain degree of popularity in the fabrication of FPDs[3].

All-ceramic restorations are one of the most commonly used treatment options, mainly when esthetics is of utmost importance; they have perfect biocompatibility with the surrounding tissue and

**DOI:** https://doi.org/10.2186/jpr.JPR_D_22_00050

***Corresponding author:** Enas Mangoush, Itäinen Pitkäkatu 2 B PharmaCity, Turku Clinical Biomaterials Centre, University of Turku, Turku, FINLAND.

**E-mail address:** enas.mangoush@utu.fi

**Table 1.** Materials used in the study.

| Material (type) | Manufacturer | Composition (wt%, vol%) |
|---|---|---|
| SFRC CAD (CAD/CAM) | Experimental | UDMA, TEGDMA, Short glass fiber (200-300 μm & Ø7 μm), Barium glass 77 wt% |
| IPS e-max CAD (CAD/CAM) | Ivoclar Vivadent AG, Schaan Liechtenstein | Silicon dioxide 57-80 wt%, Lithium oxide 11-19 wt%, Potassium oxide 0-13 wt%, Phosphorus oxide 0-11 wt% and other oxides (70 vol%). |
| TEMP PRINT medium (3D printed) | GC Corp, Tokyo, Japan | UDMA, dimethacrylate, inorganic silica fillers < 25 wt% |
| Gradia Plus (Conventional laboratory) | GC Corp, Tokyo, Japan | UDMA, dimethacrylate, inorganic fillers (71 wt%), Prepolymerized fillers (6 wt%) |
| everX Flow (SFRC/Chair-side) | GC Corp, Tokyo, Japan | Bis-EMA, TEGDMA, UDMA, Short glass fiber (200-300 μm & Ø7 μm), Barium glass (70 wt%, 46 vol%) |

TEGDMA, triethylene glycol dimethacrylate; UDMA, urethane dimethacrylate; Bis-EMA, Ethoxylated bisphenol-A-dimethacrylate; wt%, weight percentage; vol% volume percentage.

favorable optical properties[5,6]. However, they have drawbacks such as brittleness and tendency toward catastrophic failures, which are difficult to repair, and they cause wear to the opposing natural teeth if not appropriately polished[7]. For instance, clinical studies have shown that lithium-disilicate IRFPDs have a low probability of survival (5-year survival rate was 57%, 8-year survival rate decreased dramatically to 38%, and 15-year survival rate was 22%)[3,7]; however, the material has been developed extensively since then, which may influence the significance of these findings.

These clinical complications have been the mainstay of attempts to develop alternative materials with improved mechanical properties. Composite computer-aided design/computer-aided manufacturing (CAD/CAM) blocks are an alternative technique used to fabricate indirect restorations. A major advantage of composite CAD/CAM over light-polymerized conventional composites is the intensified monomer conversion attained through the high-pressure and high-temperature polymerization process[8]. Composites cause less wear on cutting equipment and are less susceptible to chipping during milling than ceramic CAD/CAM[9]. Furthermore, the composite CAD/CAM restoration repair process is more straightforward than that of ceramic restorations[8]. However, major concerns exist regarding their long-term clinical performance, as their mechanical properties are inferior to ceramics[10].

Short fiber-reinforced composites (SFRCs) have been developed to improve the mechanical properties of conventional particulate-filled composites and decrease complications that might negatively affect the long-term clinical success[11–13]. Experimental SFRC CAD/CAM composites have previously demonstrated promising performance when their mechanical, optical, surface, and bonding properties have been tested[14–16]. Concurrently, no data are available on the fracture behavior of this material when it is used to fabricate IRFPDs. Therefore, the present study aimed to assess the fracture behavior of IRFPDs made of SFRC CAD/CAM composites before and after cyclic fatigue aging compared with commercially available lithium-disilicate CAD/CAM, 3D-printed composites, conventional laboratory composites, and flowable SFRC composites. It was hypothesized that both the material type and aging procedure have no effect on the fracture behavior of the tested IRFPDs.

## 2. Materials and Methods

The materials used in this study are listed in **Table 1**.

### *2.1. Fabrication of IRFPD specimens*

One hundred laboratory-made IRFPDs with the same dimensions were fabricated using a cobalt-chromium model (**Fig. 1**). The

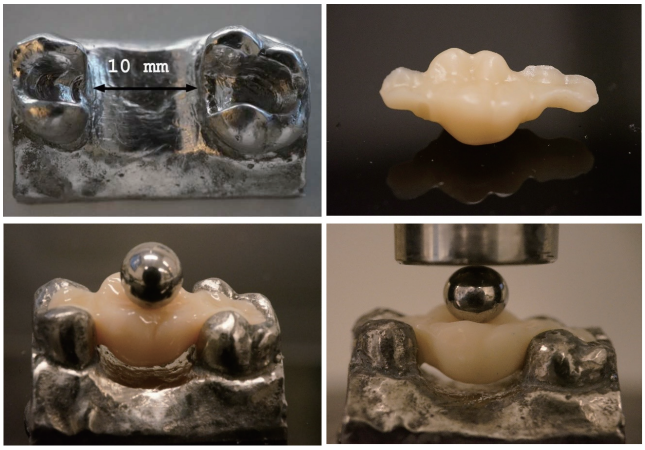


**Fig. 1.** Photographs of metal model, test specimen, and loading test setup. The mesio-occlusal inlay preparation on the 2nd molar (step: 4×2 mm; box: 3×5 mm; depth: 1.5 mm) and the disto-occlusal inlay preparation on the 2nd premolar (step: 3×2 mm; box: 2.5×3 mm; depth: 1.5 mm), with a 2-mm free space underneath the pontic.

designed metal model was cut from a cobalt-chromium blank (Sintermetall, Zirkonzahn GmbH, Taufers, Italy) using a CAD/CAM device (5-TEC, Zirkonzahn GmbH). The model was sintered in a furnace (Zirkonofen 700/UV, Zirkonzahn GmbH) according to the manufacturer's instructions. The mesio-occlusal inlay preparation (5° taper) on the second molar (step: 4×2 mm; box: 3×5 mm; depth: 1.5 mm) and the disto-occlusal inlay preparation on the second premolar (step: 3×2 mm; box: 2.5×3 mm; depth: 1.5 mm) were prepared. A distance of 10 mm was maintained between the two abutments, as it simulated the crown dimension of the mandibular first molar. A digital impression of the metal model was obtained using another dental CAD/CAM device (CEREC Omnicam AC, Dentsply Sirona, York, PA, USA). A three-unit IRFPD from the second premolar to the second molar, replacing the missing first molar (9.5 mm buccolingual and 10 mm mesiodistal width), was designed (**Fig. 1**).

A total of 100 single-structure IRFPDs were allocated to five groups (n=20/group) according to their fabrication methods and materials. The groups were as follows: specimens in the first group were experimental SFRC CAD/CAM blocks, the second group comprised specimens made of lithium-disilicate ceramic (CEREC) CAD/CAM (IPS e.max CAD, IVOCLAR), the third group comprised specimens made of 3D-printed composite (Temp PRINT, GC) using a digital light processing printer (Asiga Max UV, Asiga), and specimens in the fourth and fifth group were manually made by a build-up of conventional laboratory composite (Gradia Plus, GC) and flowable SFRC (everX Flow,

**Table 2.** Mean values of load-bearing capacity (N) and standard deviation (SD) of tested IRFPDs before and after cyclic fatigue aging. Same letters indicate no statistical significant differences between groups.

| | SFRC CAD | e-max CAD | TEMP PRINT | Gradia Plus | everX Flow |
|---|---|---|---|---|---|
| Before aging | 2624 ±463$^{d}$ | 2288 ±401$^{cd}$ | 1450 ±17$^{a}$ | 1427 ±409$^{a}$ | 2521 ±371$^{cd}$ |
| After aging | 2775 ±297$^{d}$ | 2086 ±366$^{bc}$ | 1134 ±191$^{a}$ | 1599 ±397$^{ab}$ | 2404 ±357$^{cd}$ |

GC) composites, respectively. For groups 4 and 5, a transparent template matrix (Memosil 2, Heraeus Kulzer GmbH) of an IRFPD was used to aid the fabrication of standardized restorations. First, the composite was injected into the template through three holes where the tip of the composite syringe was inserted, and the IRFPD specimen was molded. This was followed by light-curing (through the transparent silicone template) from all directions using a hand-light-curing unit (Elipar DeepCure-L, 3M ESPE) for 40 s per segment (light wavelength of 430–480 nm and light intensity of 1240 mW/cm$^2$). The light source was placed in close contact (1–2 mm) with the surface of the composite. The IRFPD specimens were then removed by cutting the silicone template horizontally with a scalpel. According to the manufacturer's instructions, the Gradia Plus restorations were polymerized in a light-curing oven (Targis Power, Ivoclar Vivadent) for 20 min.

Before cementation, the inner surface of e.max CAD IRFPDs was acid-etched (<5%) using hydrofluoric acid (IPS Ceramic etching gel, Ivoclar Vivadent) for 20 s, followed by washing, air-drying, and the application of a universal bonding agent (Scotchbond Universal, 3M ESPE). The inner surfaces of the other IRFPDs were only treated with a universal bonding agent. The restorations were then cemented to sandblasted metal abutments using a dual-cure resin cement (RelyX Ultimate, 3M ESPE). After removal of the excess material, light-curing was performed in all directions for 40 s using Elipar DeepCure-L. Prior to fatigue aging and testing, all the crowns were stored dry for 24 h at 37°C.

### *2.2. Fracture load test*

Half of the IRFPDs in each group (n=10) were subjected to cyclic fatigue aging prior to the static fracture load test. The metal model was fixed in a water bath and placed in a universal testing machine Z010 (Zwick/Roell, Ulm, Germany). The IRFPDs underwent 10,000 cycles of mechanical dynamic loading with a force of magnitude Fmax=500 N for 20 s and a frequency of 1.2 Hz. After cyclic fatigue aging, a quasi-static load was directly applied to the other half of the IRFPDs in each group (n=10/group) using a universal testing machine (Lloyd model LRX, Lloyd Instruments Ltd, Fareham, UK) at a speed of 1 mm/min. Loading was applied vertically between the triangular ridges of the buccal and lingual cusps (**Fig. 1**) using a metal ball (Ø5 mm). The loading event was registered until the restoration fractured (final drop in the load-deflection curve), and two investigators analyzed the fracture mode for each IRFPD specimen.

### *2.3. Fracture mode analysis*

The fracture mode of the IRFPDs was observed both visually and under a stereomicroscope (Heerbrugg M3Z, Heerbrugg, Switzerland) with different illumination angles and magnifications (6.5 and 15×). Two independent examiners agreed on the failure type, location, and direction. For fractographic evaluation, representative fractured IRFPD specimens were examined using scanning electron microscopy (SEM) (LEO, Oberkochen, Germany). All specimens were cleaned with ethanol and then coated with a gold layer using a sputter coater in a vacuum evaporator (BAL-TEC SCD 050 Sputter Coater, Balzers, Liechtenstein) prior to observation. The analysis started from the edge of the fractured IRFPD specimens from the upper loading surfaces to the inner structures.

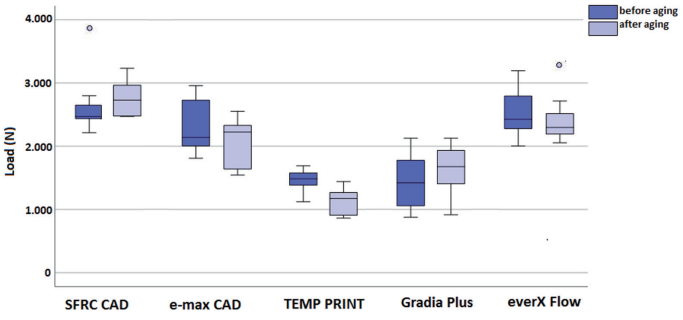


**Fig. 2.** Boxplot representing load-bearing capacity (N) values of tested IRFPDs before and after cyclic fatigue aging. Outliers' data points are presented by (◦).

### *2.4. Statistical analysis*

Statistical analysis of the data was performed using a two-way analysis of variance (ANOVA) followed by the Tukey honestly significant difference test HSD (α=.05) to assess the differences between the ultimate failure load of the IRFPDs of the groups using SPSS version 23 (SPSS, IBM Corp., NY, USA). Fracture load values were the dependent variables, while the material type and aging procedure were the independent variables. Levene's test was used to test for normal variation in outcomes.

## 3. Results

The mean values of the load-bearing capacity with the standard deviation of the tested IRFPDs before and after cyclic fatigue aging are shown in **Table 2** and **Figure 2**. Levene's test revealed that the variances were homogenous and equal across groups. ANOVA demonstrated that only the material type had a significant effect ($p$<0.05) on the load-bearing capacity values of the IRFPDs. The experimental SFRC CAD/CAM specimens exhibited the highest load-bearing capacities before and after aging among the tested groups. However, there was no significant difference ($p$>0.05) between the everX Flow group before and after aging and the e-max CAD group before aging (**Table 2**, **Fig. 2**).

After cyclic fatigue aging, the load-bearing capacity values of the experimental SFRC CAD/CAM and conventional laboratory composite (Gradia Plus) IRFPDs increased ($p$>0.05), whereas in the other three groups, the load-bearing capacity values decreased slightly after aging ($p$>0.05) (**Table 2**). The data revealed that after applying

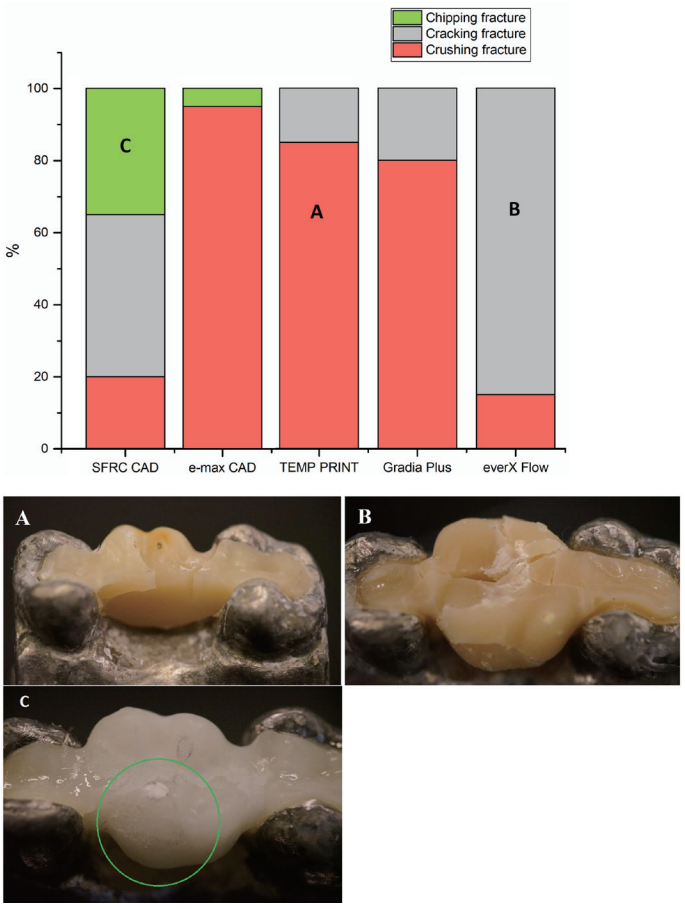


**Fig. 3.** Percentage and photographs of various fracture patterns of the restorations. (A) refers to crushing fracture, (B) refers to cracking fracture, and (C) refers to chipping fracture.

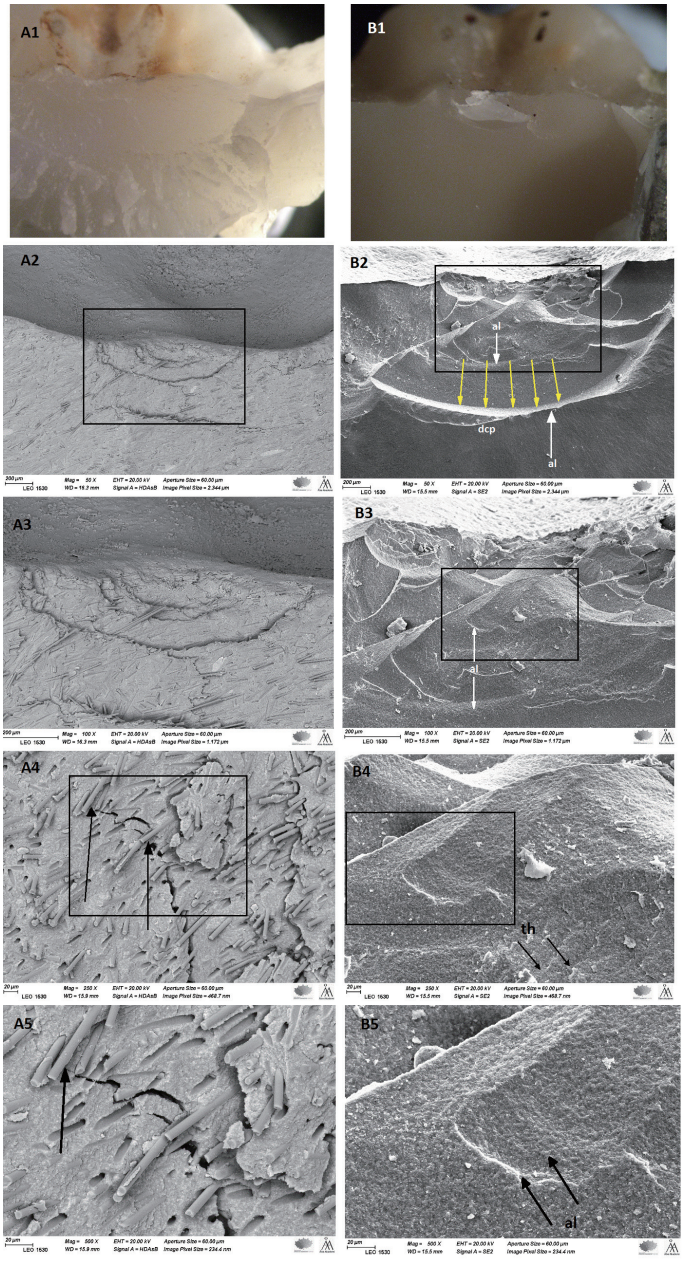


**Fig. 4.** Stereomicroscope and scanning electron microscopy images of the fractured specimens (SFRC CAD/CAM specimen **A1–5** and lithium-disilicate specimen **B1–5**) observed under different magnifications (50, 100, 250, and 500×). Arrows (A4 and A5) indicate short fibers' ability to re-direct and hinder crack propagation. (al) refers to arrest lines, (dcp) is the direction of crack propagation (yellow arrows), and (th) refers to twist hackles.

cyclic fatigue aging, the difference between the load-bearing capacity of SFRC CAD/CAM IRFPDs and e-max CAD IRFPDs was statistically significant ($p<0.05$) (**Table 2**). No statistically significant differences ($p>0.05$) were found between IRFPDs made of the 3D-printed composite (Temp PRINT) and conventional laboratory (Gradia Plus) composite before and after cyclic fatigue aging (**Table 2**). None of the restorations failed adhesively, despite the application of high loading forces. Visual inspection of the specimens revealed three different IRFPD fracture patterns (**Fig. 3**). Crushing fracture pattern (**Fig. 3A**) occurred predominantly in the 3D-printed composite, conventional flowable composite, and lithium-disilicate CAD/CAM IRFPDs groups. This type is a catastrophic fracture that cannot be repaired, where the pontic is completely crushed. Cracking (irreparable, **Fig. 3B**) and chipping (repairable, **Fig. 3C**) fracture patterns were dominant in the experimental SFRC CAD/CAM IRFPD group. In the cracking fracture, the specimen parts were not separated from each other, although many cracks were present, this type of fracture type occurred in more than 80% of specimens of the flowable SFRC IRFPDs.

**Figure 4** shows the stereomicroscope and SEM images of the fractured parts of the experimental SFRC and lithium disilicate CAD/CAM IRFPDs. The experimental SFRC CAD/CAM specimen images (different magnifications) show how the crack line propagated and was then deflected by fibers, which finally resisted further crack propagation. The lithium-disilicate specimen images (different magnifications) show fracture markers, with arrest lines (al) that appear as multiple concave lines representing the direction of the crack propagation radially downwards. Moreover, the images show fine twist hackles originating between the arrest lines.

## 4. Discussion

The present study showed that material type had a considerable effect, while aging had a non-significant effect on the fracture behavior of the tested IRFPDs; therefore, the study hypothesis was partially rejected.

Our results demonstrate that the highest load-bearing capacity values were obtained from the experimental SFRC CAD/CAM IRFPDs. According to previous research, this likely interpretation could be due to two factors. First, stress can transfer from the polymer matrix to the glass fibers, leading to higher load-bearing capacity values. Second, the glass fibers deflect the cracks individually in improving the material fracture behavior, thereby increasing the energy needed for crack propagation through the polymer matrix[17–23]. The results showed lower load-bearing capacity values for the lithium-disilicate CAD/CAM IRFPDs than for the experimental SFRC CAD/CAM composite, with a statistically significant difference after cyclic aging. These results are in accordance with other studies, which stated that composites could be more fatigue-resistant under cyclic fatigue loading than some ceramic types such as feldspathic and lithium-disilicate, especially when limited thickness is applied[24–26]. Furthermore, they reported the probability of ceramic restorations manifesting increased cyclic stresses when a cyclic loading test was applied under wet conditions[26]. Composite FPDs are resilient and can withstand loading by diffusing destructive fracture energy and undergoing more elastic deformation before failure to a greater degree than stiffer ceramic FPDs[27].

Furthermore, in a deeper look at the material properties level, fracture toughness (FT), as explained by Lassila et al., is a mechanical property that describes the resistance of brittle materials to the catastrophic propagation of flaws under an applied load[12]. Thus, it describes the damage tolerance of the material and can be considered a measure of fatigue resistance. For example, in our previous study[15], experimental SFRC blocks exhibited a mean FT value of 2.9 MPa $m^{1/2}$. In comparison, the reported FT value of the lithium-disilicate CAD/CAM (e-max CAD) in the literature was around 1.88 MPa $m^{1/2}$; these values could also explain our results[28].

The variation in the load-bearing capacity values between the experimental SFRC CAD/CAM and flowable SFRC composites, despite having similar glass fiber contents, is probably due to the differences in the amount of particulate filler content. Glass barium particles were more abundantly available in the experimental SFRC CAD/CAM (77 wt%) than in the flowable SFRC (70 wt%). Furthermore, the experimental SFRC CAD/CAM was subjected to heat curing at a high temperature and pressure. These optimum curing conditions can improve polymer cross-linking and decrease the size and number of internal defects, which consequently increases its load-bearing capacity[8,29].

Interestingly, the load-bearing capacities of the experimental SFRC CAD/CAM IRFPDs were slightly higher than those of the same material before aging. The placement of the specimens in the water path during the aging process could potentially explain these results. Under aqueous conditions, the composite matrix absorbs water, which facilitates plasticization[30]. This phenomenon could cause blunting and lower stress concentration owing to residual compressive stress generation at the fatigue crack tips. Moreover, it causes the release of accumulated tensile stress during polymerization shrinkage. These effects, either separately or combined, can hinder crack propagation, which consequently results in higher load-bearing capacity[30]. Our results are in line with those of other studies by Takeshige et al. and Wendler et al., which revealed that fatigue cracks in composites are less likely to be initiated in aqueous environments; moreover, the propagation of fatigue cracks can be retarded[30,31]. This possible hypothesis could also explain why the aged laboratory conventional composites utilized in this investigation had higher load-bearing capacity than the non-aged group of the same material. However, the plasticization effect on the fracture properties of the composites is debatable, as other studies had dissimilar findings; they showed that the aqueous environment causes degradation of the polymer chain and compromises the composite capacity to resist crack propagation[31,32]. Cyclic fatigue aging negatively affected the load-bearing capacity values of the IRFPDs made of lithium-disilicate CAD/CAM, 3D-printed composite, and flowable SFRC composite groups. The 3D-printed composite used in this study is intended for clinical interim use. It has a low content of inorganic particulate fillers (<25 wt%); thus, it is not unexpected for it to have the lowest load-bearing capacity after aging.

None of the IRFPDs failed adhesively although high loading forces were applied, reflecting a sufficient level of bonding. Visual analysis of the fracture behavior of the experimental SFRC CAD/CAM IRFPDs revealed that cracking and chipping fracture patterns were predominant (**Fig. 3**). In fractured specimens, clear surface and subsurface damage was present at the occlusal area owing to the loading process. However, there was no evidence of an association between the damaged surfaces and primary origin of the crack. According to previous studies, the weakest link of the IRFPDs lies in the connector region between the abutment and pontic, where most fractures typically occur[33,34], which could also be the origin of cracks in our specimens. The fracture path in the experimental SFRC IRFPD specimens was blocked by discontinuous fibers, which acted as stoppers and hindered further crack propagation (**Fig. 4A**); this behavior is clearly visualized in SEM images. Fibers impede the extension of a crack and develop interlocking bridges behind the progressing crack, dissipating energy by fiber pullout, resulting in graceful rather than catastrophic failure, which retains the original shape of the restoration despite the presence of multiple cracks.

In lithium-disilicate ceramics, elongated disilicate crystals (70 vol%) are tightly interlocked and homogenously distributed within the glass matrix; therefore, the crystals may hinder crack propagation. However, the cracks can still propagate through the glassy matrix[35]. Visual examination showed that the fracture mode of the lithium-disilicate IRFPD specimens was primarily catastrophic crushing-like fractures. SEM images show a radial distribution of the crack lines propagated from the loading area to the deeper structure (**Fig. 4B**). In the present investigation, the cracks in the lithium-disilicate specimen appeared to originate from the connector area (**Fig. 3**) and then propagated towards the loading area on the pontic.

Furthermore, a secondary crack emerged at the occlusal surface of the pontic, indicating that the fracture path connected the weakest connector area with the occlusal loading area as a consequence of the occlusal loading forces. Our findings are consistent with those of other investigations[33,35–39], which showed that the connector area in the lithium-disilicate IRFPD was the weakest part in which the tensile stress peaked. Fractographic markers, such as twist hackle and arrest lines, are clearly displayed in SEM images (**Fig. 4B2–5**). According to Scherrer et al., arrest lines are good indicators of the direction of crack propagation because the beginning of a crack event is frequently located on the concave side of the first arrest line[40].

Normal masticatory loads range from 98 N to 450 N, whereas the load on the FPDs during chewing varies between 125 and 290 N[27,41]. Almost all IRFPDs tested in this study under quasistatic loading survived higher loading forces than the forces mentioned above. However, restorations in the biological environment are affected by

other factors, such as inconsistent pH, enzymatic and bacterial challenges, temperature changes, cement failure, and multiple loading directions, which might collectively cause failure[41].

One of the limitations of the current study is the limited number of fatigue cycles although the same protocol was used previously[24]. The fatigue test in this study included a cyclic dynamic loading applied for 10,000 cycles, which corresponds to a short simulated clinical service time. However, the mechanical dynamic loading used with a force of magnitude 500 N is considered a high force that is not frequently reached in normal masticatory conditions. Furthermore, the cobalt-chromium models used in the present study were not able to completely reproduce the complexity of the surrounding tissue in the clinical situation as they are rigid and have an elastic modulus higher than that of dentin. In addition, the absence of tooth movement that would occur within the periodontal ligament could affect the accuracy of our results and clinical predictability of the tested materials. However, the cobalt-chromium model was chosen because it helps standardize the restorations and makes the material type the sole variable factor.

The effect of long-term water storage on the fracture behavior of the tested material combinations has not been studied; however, previous research has reported that water storage causes weakening and softening of the matrix due to water absorption by the resin component[42].

Therefore, it is essential to emphasize that this in vitro study setup cannot directly reflect in vivo conditions with a far more complex parameter setting. Using extracted teeth as abutments is preferable for testing the fracture behavior of restorations, and when assessing the material's fracture properties, fatigue loading that simulates the wear mechanism and temperature changes within the oral environment is preferable[42].

Thus, to mimic the clinical situation, fatigue with a greater number of cycles, long-term water storage, thermocycling, and loading on extracted teeth should be considered in future research. Other bridge designs, such as cantilever bridges, will provide a better understanding of the experimental material.

## 5. Conclusion

CAD/CAM-fabricated IRFPDs made of experimental SFRC blocks have shown promising performance in clinical testing in terms of fracture behavior.

## Acknowledgment

We are grateful to the manufacturing companies that provided testing materials.

## Conflict of interest

All authors confirm no economic benefits or financial interest in reporting. VP declares that he is a consultant for the Stick Tech Member of GC Company in training, research, and development. The authors declare that they have no conflicts of interest.

## References

[1] Garoushi S, Shinya A, Shinya A, Vallittu PK. Hybrid type anterior fibre-reinforced composite resin prosthesis: a case report. Eur J Prosthodont Restor Dent. 2008;16:45–7. PMID:18468325

[2] Kılıçarslan MA, Sema Kedici P, Cenker Küçükeşmen H, Uludağ BC. In vitro fracture resistance of posterior metal-ceramic and all-ceramic inlay-retained resin-bonded fixed partial dentures. J Prosthet Dent. 2004;92:365–70. https://doi.org/10.1016/j.prosdent.2004.07.001, PMID:15507910

[3] Harder S, Wolfart S, Eschbach S, Kern M. Eight-year outcome of posterior inlay-retained all-ceramic fixed dental prostheses. J Dent. 2010;38:875–81. https://doi.org/10.1016/j.jdent.2010.07.012, PMID:20691750

[4] Kois DE, Isvilanonda V, Chaiyabutr Y, Kois JC. Evaluation of fracture resistance and failure risks of posterior partial coverage restorations. J Esthet Restor Dent. 2013;25:110–22. https://doi.org/10.1111/jerd.12018, PMID:23617385

[5] Hallmann L, Ulmer P, Gerngross MD, Jetter J, Mintrone M, Lehmann F, *et al.* Properties of hot-pressed lithium silicate glass-ceramics. Dent Mater. 2019;35:713–29. https://doi.org/10.1016/j.dental.2019.02.027, PMID:30853210

[6] Zarone F, Ferrari M, Mangano FG, Leone R, Sorrentino R. Digitally oriented materials, focus on lithium dislocate ceramics. Int J Dent. 2016;2016:1–10. https://doi.org/10.1155/2016/9840594, PMID:27635140

[7] Becker M, Chaar MS, Garling A, Kern M. Fifteen-year outcome of posterior all-ceramic inlay-retained fixed dental prostheses. J Dent. 2019;89:103174. https://doi.org/10.1016/j.jdent.2019.07.012, PMID:31362035

[8] Nguyen JF, Migonney V, Ruse ND, Sadoun M. Resin composite blocks via high-pressure high-temperature polymerization. Dent Mater. 2012;28:529–34. https://doi.org/10.1016/j.dental.2011.12.003, PMID:22230107

[9] Giordano R. Materials for chairside CAD/CAM–produced restorations. J Am Dent Assoc. 2006;137(suppl):14S–21S. https://doi.org/10.14219/jada.archive.2006.0397, PMID:16950933

[10] Belli R, Wendler M, de Ligny D, Cicconi MR, Petschelt A, Peterlik H, *et al.* Chairside CAD/CAM materials. Part 1: measurement of elastic constants and microstructural characterization. Dent Mater. 2017;33:84–98. https://doi.org/10.1016/j.dental.2016.10.009, PMID:27890354

[11] Lassila L, Säilynoja E, Prinssi R, Vallittu PK, Garoushi S. Fracture behavior of Bi-structure fiber-reinforced composite restorations. J Mech Behav Biomed Mater. 2020;101:103444. https://doi.org/10.1016/j.jmbbm.2019.103444, PMID:31561057

[12] Lassila L, Keulemans F, Säilynoja E, Vallittu PK, Garoushi S. Mechanical properties and fracture behavior of flowable fiber reinforced composite restorations. Dent Mater. 2018;34:598–606. https://doi.org/10.1016/j.dental.2018.01.002, PMID:29366493

[13] Fráter M, Sáry T, Jókai B, Braunitzer G, Säilynoja E, Vallittu PK, *et al.* Fatigue behavior of endodontically treated premolars restored with different fiber-reinforced designs. Dent Mater. 2021;37:391–402. https://doi.org/10.1016/j.dental.2020.11.026, PMID:33353735

[14] Mangoush E, Lassila L, Vallittu PK, Garoushi S. Shear-bond strength and optical properties of short fiber-reinforced CAD/CAM composite blocks. Eur J Oral Sci. 2021;129:e12815. https://doi.org/10.1111/eos.12815, PMID:34322917

[15] Mangoush E, Garoushi S, Vallittu PK, Lassila L. Influence of Short Fiber- Reinforced Composites on Fracture Resistance of Single-Structure Restorations. Eur J Prosthodont Restor Dent. 2020;28:189–98. PMID:32786179

[16] Mangoush E, Lassila L, Vallittu PK, Garoushi S. Microstructure and Surface Characteristics of Short- Fiber Reinforced CAD/CAM Composite Blocks. Eur J Prosthodont Restor Dent. 2021;29. PMID:33508179

[17] Garoushi S, Säilynoja E, Vallittu PK, Lassila L. Physical properties and depth of cure of a new short fiber reinforced composite. Dent Mater. 2013;29:835–41. https://doi.org/10.1016/j.dental.2013.04.016, PMID:23726127

[18] Garoushi S, Vallittu PK, Lassila LVJ. Short glass fiber reinforced restorative composite resin with semi-inter penetrating polymer network matrix. Dent Mater. 2007;23:1356–62. https://doi.org/10.1016/j.dental.2006.11.017, PMID:17204319

[19] Nagata K, Garoushi SK, Vallittu PK, Wakabayashi N, Takahashi H, Lassila LVJ. Fracture behavior of single-structure fiber-reinforced composite restorations. Acta Biomater Odontol Scand. 2016;2:118–24. https://doi.org/10.1080/23337931.2016.1224670, PMID:28642921

[20] Garoushi S, Vallittu PK, Lassila LVJ. Direct restoration of severely damaged incisors using short fiber-reinforced composite resin. J Dent. 2007;35:731–6. https://doi.org/10.1016/j.jdent.2007.05.009, PMID:17614187

[21] Göncü Başaran E, Ayna E, Vallittu PK, Lassila LVJ. Load-bearing capacity of handmade and computer-aided design–computer-aided manufacturing-fabricated three-unit fixed dental prostheses of particulate filler composite. Acta Odontol Scand. 2011;69:144–50. https://doi.org/10.3109/00016357.2010.545034, PMID:21208023

[22] Cekic-Nagas I, Egilmez F, Ergun G, Vallittu PK, Lassila LVJ. Load-bearing capacity of novel resin-based fixed dental prosthesis materials. Dent Mater J. 2018;37:49–58. https://doi.org/10.4012/dmj.2016-367, PMID:29081445

[23] Başaran EG, Ayna E, Vallittu PK, Lassila LVJ. Load bearing capacity of fiber-reinforced and unreinforced composite resin CAD/CAM-fabricated fixed dental prostheses. J Prosthet Dent. 2013;109:88–94. https://doi.org/10.1016/S0022-3913(13)60022-0, PMID:23395334

[24] Belli R, Geinzer E, Muschweck A, Petschelt A, Lohbauer U. Mechanical fatigue degradation of ceramics versus resin composites for dental restorations. Dent Mater. 2014;30:424–32. https://doi.org/10.1016/j.dental.2014.01.003, PMID:24553249

[25] Hamburger JT, Opdam NJM, Bronkhorst EM, Huysmans MCDNJM. Indirect restorations for severe tooth wear: fracture risk and layer thickness. J Dent. 2014;42:413–8. https://doi.org/10.1016/j.jdent.2013.10.003, PMID:24120523

[26] Kassem AS, Atta O, El-Mowafy O. Fatigue resistance and microleakage of CAD/CAM ceramic and composite molar crowns. J Prosthodont. 2012;21:28–32. https://doi.org/10.1111/j.1532-849X.2011.00773.x, PMID:22008462

[27] Awada A, Nathanson D. Mechanical properties of resin-ceramic CAD/CAM restorative materials. J Prosthet Dent. 2015;114:587–93. https://doi.org/10.1016/j.prosdent.2015.04.016, PMID:26141648

[28] Badawy R, El-Mowafy O, Tam LE. Fracture toughness of chairside CAD/CAM materials – Alternative loading approach for compact tension test. Dent Mater. 2016;32:847–52. https://doi.org/10.1016/j.dental.2016.03.003, PMID:27133875

[29] Nguyen JF, Migonney V, Ruse ND, Sadoun M. Properties of experimental urethane dimethacrylate-based dental resin composite blocks obtained via thermo-polymerization under high pressure. Dent Mater. 2013;29:535–41. https://doi.org/10.1016/j.dental.2013.02.006, PMID:23522657

[30] Takeshige F, Kawakami Y, Hayashi M, Ebisu S. Fatigue behavior of resin composites in aqueous environments. Dent Mater. 2007;23:893–9. https://doi.org/10.1016/j.dental.2006.06.031, PMID:17007919

[31] Wendler M, Stenger A, Ripper J, Priewich E, Belli R, Lohbauer U. Mechanical degradation of contemporary CAD/CAM resin composite materials after water ageing. Dent Mater. 2021;37:1156–67. https://doi.org/10.1016/j.dental.2021.04.002, PMID:33933272

[32] Lohbauer U, Belli R, Ferracane JL. Factors involved in mechanical fatigue degradation of dental resin composites. J Dent Res. 2013;92:584–91. https://doi.org/10.1177/0022034513490734, PMID:23694927

[33] Kolbeck C, Rosentritt M, Behr M, Lang R, Handel G. In vitro examination of the fracture strength of 3 different fiber-reinforced composite and 1 all-ceramic posterior inlay fixed partial denture systems. J Prosthodont. 2002;11:248–53. PMID:12501138

[34] Fischer H, Weber M, Eck M, Erdrich A, Marx R. Finite element and experimental analyses of polymer-based dental bridges reinforced by ceramic bars. J Biomech. 2004;37:289–94. https://doi.org/10.1016/j.jbiomech.2003.08.013, PMID:14757447

[35] Zarone F, Di Mauro MI, Ausiello P, Ruggiero G, Sorrentino R. Current status on lithium disilicate and zirconia: a narrative review. BMC Oral Health. 2019;19:134. https://doi.org/10.1186/s12903-019-0838-x, PMID:31272441

[36] Wolfart S, Ludwig K, Uphaus A, Kern M. Fracture strength of all-ceramic posterior inlay-retained fixed partial dentures. Dent Mater. 2007;23:1513–20. https://doi.org/10.1016/j.dental.2006.12.006, PMID:17368743

[37] Puschmann D, Wolfart S, Ludwig K, Kern M. Load-bearing capacity of all-ceramic posterior inlay-retained fixed dental prostheses. Eur J Oral Sci. 2009;117:312–8. https://doi.org/10.1111/j.1600-0722.2009.00626.x, PMID:19583761

[38] Saridag S, Ozyesil AG, Pekkan G. Fracture strength and bending of all-ceramic and fiber-reinforced composites in inlay-retained fixed partial dentures. J Dent Sci. 2012;7:159–64. https://doi.org/10.1016/j.jds.2012.03.013

[39] Zhang Z, Thompson M, Field C, Li W, Li Q, Swain MV. Fracture behavior of inlay and onlay fixed partial dentures – An in-vitro experimental and XFEM modeling study. J Mech Behav Biomed Mater. 2016;59:279–90. https://doi.org/10.1016/j.jmbbm.2016.01.035, PMID:26894661

[40] Scherrer SS, Quinn GD, Quinn JB. Fractographic failure analysis of a Procera® AllCeram crown using stereo and scanning electron microscopy. Dent Mater. 2008;24:1107–13. https://doi.org/10.1016/j.dental.2008.01.002, PMID:18314187

[41] Basso GR, Moraes RR, Borba M, Duan Y, Griggs JA, Bona AD. Reliability and failure behavior of CAD-on fixed partial dentures. Dent Mater. 2016;32:624–30. https://doi.org/10.1016/j.dental.2016.01.013, PMID:26897479

[42] Zimmermann M, Ender A, Egli G, Özcan M, Mehl A. Fracture load of CAD/CAM-fabricated and 3D-printed composite crowns as a function of material thickness. Clin Oral Investig. 2019;23:2777–84. https://doi.org/10.1007/s00784-018-2717-2, PMID:30368664